

Global-scale Magnetism (and Cycles) in Dynamo Simulations of Stellar Convection Zones

Benjamin P. Brown^{1,2}, Matthew K. Browning³, Allan Sacha Brun⁴, Mark S. Miesch⁵ and Juri Toomre⁶

¹*Dept. Astronomy, University of Wisconsin, Madison, WI 53706-1582*

²*Center for Magnetic Self Organization in Laboratory and Astrophysical Plasmas, University of Wisconsin, Madison, WI 537066-1582*

³*Canadian Institute for Theoretical Astrophysics, University of Toronto, Toronto, ON M5S3H8 Canada*

⁴*DSM/IRFU/SAP, CEA-Saclay and UMR AIM, CEA-CNRS-Université Paris 7, 91191 Gif-sur-Yvette, France*

⁵*High Altitude Observatory, NCAR, Boulder, CO 80307-3000*

⁶*JILA and Dept. Astrophysical & Planetary Sciences, University of Colorado, Boulder, CO 80309-0440*

Abstract. Young solar-type stars rotate rapidly and are very magnetically active. The magnetic fields at their surfaces likely originate in their convective envelopes where convection and rotation can drive strong dynamo action. Here we explore simulations of global-scale stellar convection in rapidly rotating suns using the 3-D MHD anelastic spherical harmonic (ASH) code. The magnetic fields built in these dynamos are organized on global-scales into wreath-like structures that span the convection zone. We explore one case that rotates five times faster than the Sun in detail. This dynamo simulation, called case D5, has repeated quasi-cyclic reversals of global-scale polarity. We compare this case D5 to the broader family of simulations we have been able to explore and discuss how future simulations and observations can advance our understanding of stellar dynamos and magnetism.

1. Introduction

Magnetism is a ubiquitous feature of stars like our Sun. The magnetism we see at the surface probably has its origin in stellar dynamo action arising in the convective envelopes beneath the photosphere. There, turbulent plasma motions couple with rotation to build organized fields on global-scales. These processes occur in the Sun as well and are probably the source of the 11-year activity cycle. Despite intense study, solar and stellar dynamos are poorly understood, and at present we are unable to reliably predict even large-scale features of the solar cycle.

Observations of young, rapidly rotating stars indicate that they have strong magnetic fields at their surfaces. There are clearly observed correlations between rotation and activity which appear to hold generally for stars on the lower main sequence (e.g.,

Pizzolato et al. 2003). Many of these stars show cycles of activity as well, though here the dependence on rotation rate, stellar mass and other fundamental parameters is less clear (e.g., Saar & Brandenburg 1999; Oláh et al. 2009). At present even from a theoretical perspective we do not understand how the stellar dynamo process depends in detail on rotation.

Motivated by this rich observational landscape, we have explored the effects of more rapid rotation on 3-D convection and dynamo action in simulations of stellar convection zones. These simulations have been conducted using the anelastic spherical harmonic (ASH) code to study global-scale magnetohydrodynamic convection and dynamo action in stellar convection zones (e.g., Clune et al. 1999; Miesch et al. 2000; Brun et al. 2004). In the past, global-scale convective dynamo simulations have focused primarily on the Sun, but now explorations are beginning for a variety of stars, ranging from A-type (e.g., Brun et al. 2005; Featherstone et al. 2009) to the M-type dwarfs (Browning 2008).

Here we will discuss simulations of G-type stars that rotate more rapidly than the Sun. We began these explorations by exploring convection in hydrodynamic simulations at a variety of rotation rates (Brown et al. 2008). These simulations capture the convection zone only, spanning from $0.72 R_{\odot}$ to $0.97 R_{\odot}$, and take solar values for luminosity and stratification but the rotation rate is more rapid. The total density contrast across such shells is about 25. In those simulations we found that the differential rotation generally becomes stronger as the rotation rate increases, while the meridional circulations appear to become weaker and multi-celled in both radius and latitude.

These rapidly rotating stars have vigorous dynamos, and the magnetic fields created in the dynamos are often organized on global-scales into banded wreath-like structures (Brown et al. 2010a). Surprisingly, this organization occurs in the middle of the convection zone itself, rather than in a tachocline of penetration and shear between the convection zone and stable radiative zone beneath. Many of the wreath-building undergo quasi-cyclic reversals of magnetic polarity. Here we explore one of these cyclic dynamos (§2), before putting it in context with other such dynamos (§3).

2. Wreaths and Cycles in a Stellar Convection Zone

Our main focus here is on a convective dynamo in a star rotating five times faster than our Sun currently does, which we call case D5 (Brown et al. 2010b). Vigorous convection in this simulation drives a strong differential rotation, which in turns fuels a strong dynamo. The magnetic fields created in this dynamo are organized on global-scales into banded wreath-like structures, as shown in Figure 1a. Two wreaths are visible near the equator, spanning the depth of the convection zone and latitudes from roughly $\pm 30^{\circ}$. The longitudinal field B_{ϕ} dominates the magnetic structures, and the two wreaths have opposite polarities (positive in northern hemisphere, negative in the southern). Magnetic fields meander in and out of each wreath, connecting them to one another across the equator where small knots of alternating polarity are visible throughout. The wreaths are also connected to high latitudes, where magnetic structures of opposite polarity are visible; these polar structures are relic wreaths from the previous global-scale reversal.

We follow one such reversal in Figure 1. During the reversal (Fig. 1b), new wreaths of opposite polarity form near the equator and begin to grow in strength. After a reversal (Fig. 1c) the new magnetic wreaths dominate the equatorial region, while the old

wreaths propagate towards the poles. The origin of this poleward propagation appears to be a combination of a nonlinear dynamo wave, arising from systematic spatial offsets between the generation terms for mean poloidal and toroidal magnetic field, and possibly a poleward-slip instability arising from magnetic stresses within the wreaths. Life near the equator can be quite complex, and at times during the middle of the cycle states with substantial non-axisymmetry are realized (Fig. 1*d*). In the polar regions, convection begins to unravel the wreaths from the previous cycle, reconnecting them with the pre-existing flux there.

3. Wreath-building Dynamos

Case D5 is part of a much larger family of simulations that we have conducted exploring convection and dynamo action in younger suns. The properties of this broad family are summarized in Figure 2*a*. Indicated here are 26 simulations at rotation rates ranging from $0.5 \Omega_{\odot}$ to $15 \Omega_{\odot}$. At individual rotation rates (e.g., $3 \Omega_{\odot}$), further simulations explore the effects of lower magnetic diffusivity η and hence higher magnetic Reynolds numbers. Some of these follow a path where the magnetic Prandtl number Pm is fixed at 0.5 (triangles) while others sample up to $Pm=4$ (diamonds). The most turbulent simulations have fluctuating magnetic Reynolds numbers of about 500 at mid-convection zone. Wreath-building dynamos are achieved in most simulations (17), though a smaller number do not successfully regenerate their mean poloidal fields (9, indicated with crosses). Very approximate regimes of dynamo behavior are indicated, based on the time variations shown by the different classes of dynamos.

Detailed studies of cases D3 and D5 indicate that the magnetic wreaths are built by both the global-scale differential rotation and by the turbulent emf arising from correlations in the convection (Brown et al. 2010a,b). Generally, the mean longitudinal magnetic field $\langle B_{\phi} \rangle$ in the wreaths is generated by the Ω -effect: the stretching of mean poloidal field by the shear of differential rotation into mean toroidal field. Production of $\langle B_{\phi} \rangle$ by the differential rotation is typically balanced by turbulent shear and advection, and by ohmic diffusion on the largest scales.

The mean poloidal field in these simulations is generated by the turbulent emf $E_{FI} = \langle \vec{u}' \times \vec{B}' \rangle$, where the fluctuating velocity is $\vec{u}' = \vec{u} - \langle \vec{u} \rangle$ and the fluctuating magnetic fields are $\vec{B}' = \vec{B} - \langle \vec{B} \rangle$. In cases D3 and D5, E_{FI} is generally strongest at the poleward edge of the wreaths, centered at approximately $\pm 20^{\circ}$ latitude, whereas the Ω -effect and $\langle B_{\phi} \rangle$ peak at roughly $\pm 15^{\circ}$ latitude. This spatial offset between E_{FI} and $\langle B_{\phi} \rangle$ means that the turbulent emf is not generally well represented by a simple α -effect description, e.g.,

$$E_{FI} = \langle \vec{u}' \times \vec{B}' \rangle_{\phi} \neq \alpha \langle B_{\phi} \rangle \quad (1)$$

when α is a scalar quantity. This is true even when α is estimated from the kinetic and magnetic helicities present in the simulation. More sophisticated mean-field models may do much better at matching the observed emf E_{FI} , and other terms in the mean-field expansion may play a significant role; in particular, the gradient of $\langle B_{\phi} \rangle$ is large on the poleward edges of the wreaths where E_{FI} is significant. During reversals in case D5, both E_{FI} and the production of $\langle B_{\phi} \rangle$ associated with the Ω -effect surf on the poleward edge of the wreaths as those structures move poleward. This systematic phase shift appears to contribute to that propagation.

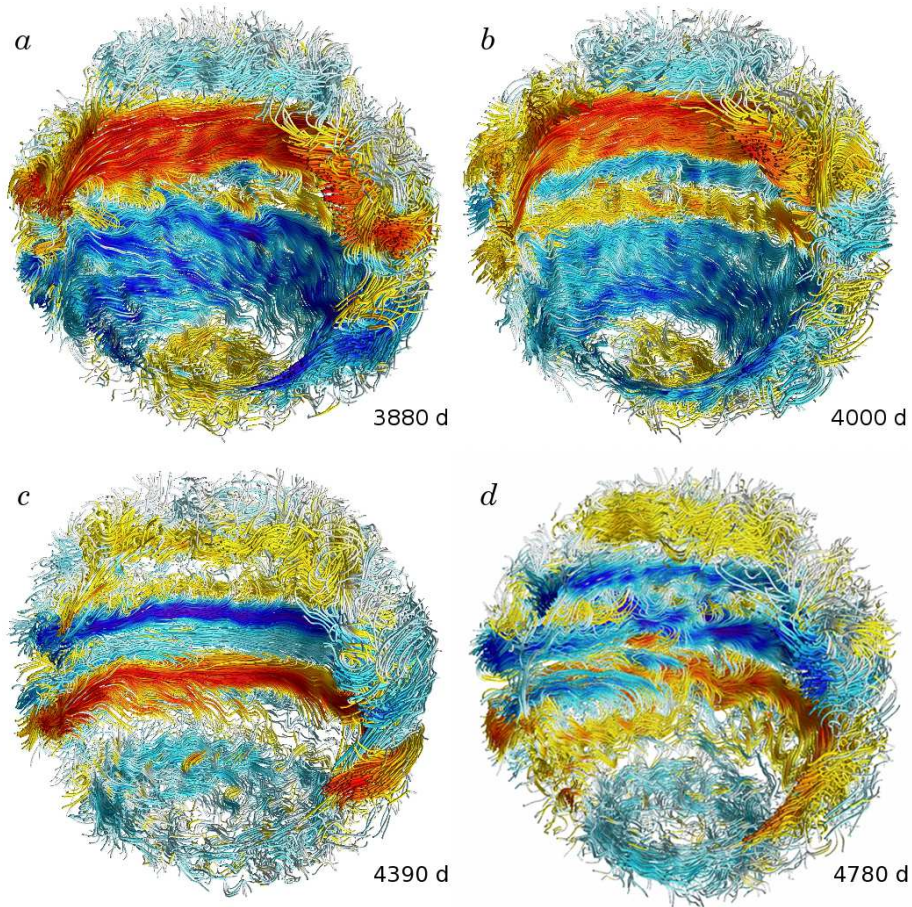


Figure 1. Tracing of fieldlines in magnetic wreaths of case D5 during a magnetic reversal; volume shown spans slightly more than a full hemisphere. (a) Shortly before a reversal, with a positive polarity wreath above the equator (red tones) and negative polarity below (blue tones). Relic wreaths from the previous cycle remain visible in the polar caps. (b) During a reversal, new wreaths with opposite polarity form at the equator. (c) When the reversal completes, the polarity of the wreaths have flipped, with negative polarity wreath above the equator and positive below. The old wreaths propagate towards the poles where they slowly dissipate. (d) Mid-cycle, complex non-axisymmetric states are sometimes attained but do not always trigger reversals. Times of snapshots are labeled, and color tables range from $\pm 25\text{kG}$, with peak fields reaching $\pm 40\text{kG}$.

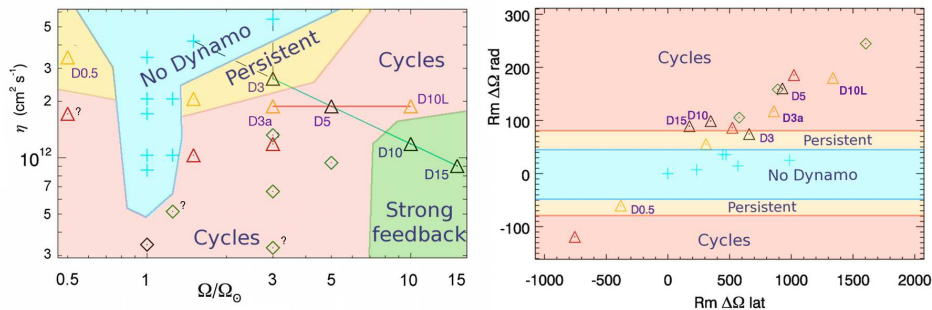


Figure 2. Parameter space explored by wreath-building dynamos. (a) Primary control parameters magnetic diffusivity η and rotation rate Ω are shown for dynamo simulations at rotation rates ranging sampling $0.5\text{--}15 \Omega_{\odot}$, with very approximate dynamo regimes shown and with some cases labeled. In some regions, magnetic Reynolds numbers are too low to sustain dynamo action, while in other regions persistent magnetic wreaths form which do not show evidence for cycles. At higher magnetic Reynolds numbers (occurring here at low η or high Ω), wreaths typically undergo quasi-cyclic reversals. At the highest rotation rates the Lorentz force can substantially modify the differential rotation, but dynamo action is still achieved. Cases marked with question marks show significant time-variation but have not been evolved for long enough to establish cyclic behavior. (b) Plot of magnetic Reynolds numbers associated with global-scale differential rotation. The dynamos are largely driven by differential rotation, and the radial shear (vertical axis) appears to discriminate between the different dynamo regimes.

As the differential rotation plays a crucial role in these dynamos, we define magnetic Reynolds numbers associated with the latitudinal shear at mid-convection zone and the radial shear across the convection zone:

$$Rm \Delta\Omega \text{ lat} = \frac{\Delta\Omega_{\text{lat}} R D}{\eta} \quad (2)$$

$$Rm \Delta\Omega \text{ rad} = \frac{\Delta\Omega_r D^2}{\eta} \quad (3)$$

were $R = 0.85R_{\odot}$ is the radial location of the mid-convection zone, $D = 0.3R_{\odot}$ is the depth of the convection zone, $\Delta\Omega_{\text{lat,r}}$ are the angular velocity contrasts in latitude and radius respectively (e.g., Brown et al. 2010a) and η is the magnetic diffusivity at mid-convection zone. These magnetic Reynolds numbers are shown in Figure 2b for many of the dynamos, neglecting some cases with very high magnetic Reynolds numbers.

The latitudinal shear is generally large in all of these dynamos (horizontal axis), and all of the simulations, including those that fail to sustain dynamo action, succeed in initially producing global-scale toroidal magnetic structures. The radial shear near the equator is relatively weaker (vertical axis), and this quantity more clearly separates those dynamos that succeed from those that fail. The radial differential rotation also discriminates the cyclic dynamos from those that build persistent fields. Somewhat surprisingly, the magnetic Reynolds number associated with the fluctuating convection does not provide as good of a discriminant between dynamos that succeed or fail. The simulations that fail to sustain dynamo action are those that do not regenerate their

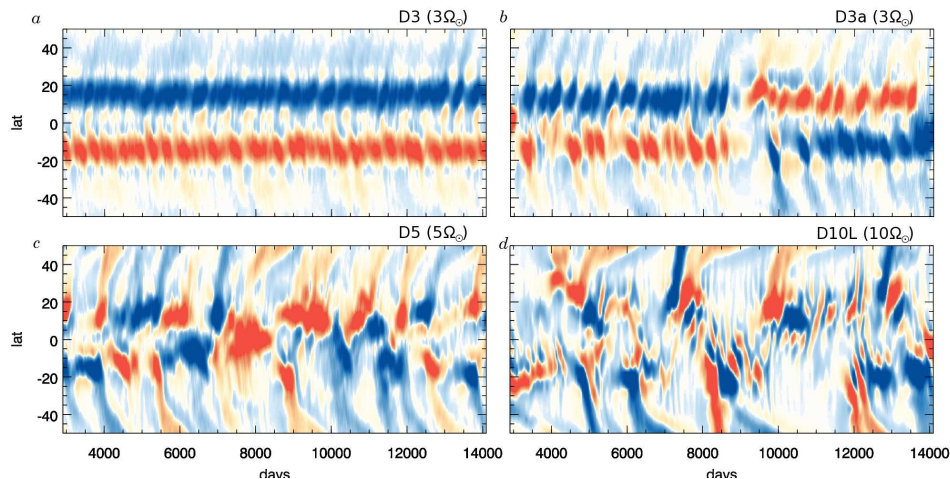


Figure 3. Mean toroidal magnetic field in four wreath-building dynamos at mid-convection zone, shown as time latitude maps. (a) Persistent case D3 with fields that do not change in sense. (b) More turbulent companion case D3a shows long cycles. (c) Cyclic case D5. (d) Case D10L.

poloidal fields quickly enough. The clear dependence on $\Delta\Omega_r$ and the weak dependence on the properties of the fluctuating convection suggest again that these wreath-building dynamos may rely on effects other than a classical α -effect to build their turbulent emf E_{FI} which generates the global-scale poloidal fields.

Two of the dynamos shown in Figure 2b have negative magnetic Reynolds numbers. These are the two slowly-spinning simulations which rotate half as quickly as our Sun currently does (e.g., case D0.5). In these simulations, the differential rotation is anti-solar in nature and opposite in sense to that of the Sun, with rapidly spinning pole and a more slowly spinning equator. Despite this fundamental difference, these simulations drive strong dynamos and build magnetic wreath-like structures in their convection zones. Anti-solar differential rotation appears to arise when convection is only slightly constrained by rotation (e.g., when the Rossby number is large), while solar-like differential rotation arises in rapidly rotating stars (when the Rossby number is small). The angular velocity shear associated with the differential rotation increases as the Rossby number becomes either large or small. The Sun itself appears to be very near Rossby number unity, and this partially explains the difficulty in attaining wreath-building dynamos in previous solar dynamo simulations: the angular velocity contrast in the Sun is smaller than that realized in the rapidly rotating dynamos. As a consequence, the solar dynamo simulations require low values of η to build wreaths, which in turn calls for high resolutions and that exacts a large computational cost.

Many of these dynamos show global-scale reversals, but the dependence of this phenomena on rotation rate or Reynolds number are somewhat unclear. Near the onset of wreath-building dynamo action we generally find little time variation in the axisymmetric magnetic fields associated with the wreaths. This is illustrated for case D3 in Figure 3a, where the mean longitudinal field $\langle B_\phi \rangle$ is shown at mid-convection zone over an interval of nearly 10,000 days. Though small variations are visible on a roughly 500 day timescale, the two wreaths retain their polarities for the entire time simulated

(more than 20,000 days), which is significantly longer than the convective overturn time (roughly 10–30 days), the rotation period (9.3 days), or the ohmic diffusion time (about 1300 days at mid-convection zone). We refer to the dynamos in this regime as persistent wreath-builders.

Generally, we find that wreath-building dynamos begin to show large time dependence as the magnetic diffusivity η decreases and as the rotation rate Ω increases. Case D3a, rotating three times the solar rate but with lower diffusivities than case D3, is an example of the first behavior and undergoes reversals even though D3 did not (Fig. 3b). To explore the dependence on rotation rate, we compare cases D3a, D5 and D10L, which have the same magnetic, momentum and thermal diffusivities but rotate at three, five and ten times the solar rate respectively. In case D5 the global-scale reversals are more frequent, occurring with a roughly 1500 day timescale (Fig. 3c), though during some intervals the dynamo can fall into other states. When we explore case D10L rotating ten times the solar rate, we find that the cycles are somewhat harder to define, with the northern and southern hemispheres showing distinctly different behavior (Fig. 3d). It is unclear at present how the cycle period depends on the rotation rate of the star; case D3a and D5 would imply that faster rotation leads to shorter cycles in general agreement with observations, but all of these simulations are highly variable and actual cycle periods are difficult to quantitatively define.

The magnetic wreaths act back strongly on the differential rotation that feeds their generation, and the global-scale shear is much weaker in dynamo simulations than in corresponding hydrodynamic simulations. Individual convective structures are largely unaffected by the magnetic wreaths except when the fields reach very large amplitudes; in case D5 this occurs when B_ϕ exceeds values of roughly 35 kG at mid-convection zone. At the highest rotation rates the Lorentz force of the axisymmetric magnetic fields becomes strong enough to substantially modify the differential rotation, largely wiping out the latitudinal and radial shear (e.g., cases D10 and D15 in Fig. 2a). In these cases, wreath-like structures can still form though they typically have more complex structure and are less axisymmetric.

4. Overview

Advances in massively parallel supercomputers are now permitting simulations that can capture global-scale convection and dynamo action in stars like our Sun. Dynamo simulations of solar-type stars are revealing that organized magnetic fields can be built in the convection zone itself, without necessarily relying on a tachocline in between the convection zone and radiative zone for this organization. This is a marked departure from many solar dynamo theories, where the tachocline plays a vital role. Many of these simulations show quasi-cyclic reversals of magnetic polarity. These cycles are not yet like the solar cycle: namely, they are typically too short and generally the magnetic fields migrate towards the poles, rather than towards the equator as observed at the solar surface (though see Ghizaru et al. 2010). Simulations remain well separated in parameter space from real stellar convection, which remains humbly out of reach for the foreseeable future, but these global-scale simulations are entering a regime where resolved turbulence plays a larger role than explicit diffusion. Thus they are beginning to capture in a self-consistent fashion the processes which likely contribute most directly to stellar dynamo action.

In the future we will be exploring convection and dynamo action in K- and F-type stars, to understand how stellar mass and convection zone depth affect the global-scale dynamo. This work will complement ongoing work exploring dynamo action in fully convective M-dwarfs (Browning 2008). As simulations move away from the Sun, we need further constraints from stellar observations. In particular, measurements of stellar differential rotation are vitally important, given the role of that global-scale flow in the wreath building dynamos. An observational understanding of how dynamo properties including magnetic activity and cyclic period scale with differential rotation would be of great utility.

Acknowledgments. We thank Nicholas Nelson for his excellent and continuing work on dynamo case D3a (Figure 3b) and its relatives. This research is supported by NASA through Heliophysics Theory Program grants NNG05G124G and NNX08AI57G, with additional support for Brown through the NSF Astronomy and Astrophysics post-doctoral fellowship AST 09-02004. CMSO is supported by NSF grant PHY 08-21899. Miesch was supported by NASA SR&T grant NNH09AK14I. NCAR is sponsored by the National Science Foundation. Browning is supported by research support at CITA. Brun was partly supported by the Programme National Soleil-Terre of CNRS/INSU (France), and by the STARS2 grant from the European Research Council. The simulations were carried out with NSF PACI support of PSC, SDSC, TACC and NCSA. Field line tracings shown in Figure 1 were produced using VAPOR (Clyne et al. 2007).

References

- Brown, B. P., Browning, M. K., Brun, A. S., Miesch, M. S., & Toomre, J. 2008, *ApJ*, 689, 1354. 0808.1716
 — 2010a, *ApJ*, 711, 424
 Brown, B. P., Miesch, M. S., Browning, M. K., Brun, A. S., & Toomre, J. 2010b, *ApJ*. submitted
 Browning, M. K. 2008, *ApJ*, 676, 1262. arXiv:0712.1603
 Brun, A. S., Browning, M. K., & Toomre, J. 2005, *ApJ*, 629, 461. arXiv:astro-ph/0610072
 Brun, A. S., Miesch, M. S., & Toomre, J. 2004, *ApJ*, 614, 1073
 Clune, T. L., Elliott, J. R., Glatzmaier, G. A., Miesch, M. S., & Toomre, J. 1999, *Parallel Computing*, 25, 361
 Clyne, J., Mininni, P., Norton, A., & Rast, M. 2007, *New Journal of Physics*, 9, 301
 Featherstone, N. A., Browning, M. K., Brun, A. S., & Toomre, J. 2009, *ApJ*, 328, 1126
 Ghizaru, M., Charbonneau, P., & Smolarkiewicz, P. K. 2010, *ApJ*, 715, L133
 Miesch, M. S., Elliott, J. R., Toomre, J., Clune, T. L., Glatzmaier, G. A., & Gilman, P. A. 2000, *ApJ*, 532, 593
 Oláh, K., Kolláth, Z., Granzer, T., Strassmeier, K. G., Lanza, A. F., Järvinen, S., Korhonen, H., Baliunas, S. L., Soon, W., Messina, S., & Cutispoto, G. 2009, *A&A*, 501, 703. 0904.1747
 Pizzolato, N., Maggio, A., Micela, G., Sciortino, S., & Ventura, P. 2003, *A&A*, 397, 147
 Saar, S. H., & Brandenburg, A. 1999, *ApJ*, 524, 295